

Parametric structural optimization with dynamic knot RBFs and partition of unity method

Hon Shan Ho · Michael Yu Wang · Mingdong Zhou

Received: 22 February 2012 / Revised: 12 August 2012 / Accepted: 12 September 2012 / Published online: 7 November 2012
© Springer-Verlag Berlin Heidelberg 2012

Abstract An efficient algorithm is presented for solving optimization problem of geometrical domains in which elliptic boundary value problems are defined. The surface of the domain is implicitly described through a level set function and the moving boundary is determined by the time-dependent dynamic knots of the radial basis functions (RBFs). A method of Partition of Unity (POU) is leveraged to calculate the solution, which divides the domain into some smaller overlapping local sub-domains and reconstructs them into the global surface with less numerical cost. Apart from the convergence properties, numerical results are given and discussed.

Keywords Structural optimization · Radial basis function · Dynamic knots · Partition of unity

1 Introduction

Numerical techniques for structural optimization have put emphasis on generality and high efficiency. A preferred

formulation should allow geometric evolution and material distribution simultaneously, and also be simple enough for developing an effective optimal solution with respect to various design constraints.

In addition to the well-established numerical methods, such as the homogenization approach (Bendsøe and Kikuchi 1988), the Solid Isotropic Microstructure with Penalization (SIMP) method (Bendsøe 1989; Bendsøe and Sigmund 2003; Rozvany et al. 1992), and the Evolutionary Structural Optimization (ESO) method (Xie and Steven 1993, 1997), the level set based approach (Allaire et al. 2004; Wang et al. 2003) excels in smooth structural boundary representation with versatility in handling both geometric and topological changes. However, the conventional level set method requires complex numerical computation, such as discretization and reinitialization, which may cause numerical artifacts and thus hinder its potential as expected.

One successful improvement is to transform the implicit level set model into a parametric RBF model, either using globally supported basis functions (Buhmann 2004; Ho et al. 2011; Lui et al. 2007; Wang and Wang 2006; Wei and Wang 2006; Xing et al. 2007), or compactly supported ones (Luo et al. 2007). This technique has been recognized as an effective tool in topology optimization. In the authors' previous work (Ho et al. 2011), two major schemes of RBF parameterizations are studied: (i) varied knots distribution algorithm, and (ii) fixed knots with POU algorithm. The dynamic knots scheme is aimed at utilizing each basis function to its maximum extent in the level set function representation. Thus, the benefit is to reduce the number of basis functions and hence the computational cost. The POU scheme restrains the span of a set of basis functions within their local region and consequently saves efforts in the sensitivity integration computations.

H. S. Ho
Department of Electrical Engineering,
The Hong Kong Polytechnic University,
Hung Hom, Kowloon, Hong Kong
e-mail: eehsho@polyu.edu.hk

M. Y. Wang (✉) · M. Zhou
Department of Mechanical and Automation Engineering,
The Chinese University of Hong Kong,
Shatin, NT, Hong Kong
e-mail: yuwang@mae.cuhk.edu.hk

M. Zhou
e-mail: mdzhou@mae.cuhk.edu.hk

In this paper, a novel method is proposed by combining the above two ideas, which aims to use the knot position of the local RBFs as the design variable within the POU scheme. Numerical experiments show that the investigation yields a concrete technique with a high level of computational efficiency and desirable capability.

This paper is organized as follows. The RBF with POU method for level set based structural optimization is reviewed briefly in Section 2. A detailed sensitivity analysis and the coupled optimization algorithm are elaborated in Section 3. Numerical experiments of different configuration settings are presented and discussed in Section 4. Finally, conclusions and future work are stated in Section 5.

2 Parametric modeling for structural optimization

2.1 Level set based structural optimization

Given a bounded design domain $D \subset \mathbb{R}^d$, which includes all admissible shapes Ω , i.e. $\Omega \subset D$, the shape and topology of underlying structure are described through a Lipschitz-continuous implicit level set function $\Phi(\mathbf{x})$ as follows:

$$\begin{aligned} \Phi(\mathbf{x}) &= 0 & \forall \mathbf{x} \in \partial\Omega \cap D, \\ \Phi(\mathbf{x}) &< 0 & \forall \mathbf{x} \in \Omega \setminus \partial\Omega, \\ \Phi(\mathbf{x}) &> 0 & \forall \mathbf{x} \in (D \setminus \Omega), \end{aligned} \quad (1)$$

where the structural interface is captured as the zero iso-surface $\{\mathbf{x} \in \mathbb{R}^d \mid \Phi(\mathbf{x}) = 0\}$ ($d = 2$ or 3). In the level set method, the dynamic interface is assumed to move only in the normal direction, and its motion is essentially governed by a Hamilton–Jacobi type equation:

$$\frac{\partial \Phi(\mathbf{x}, t)}{\partial t} + v_n \cdot |\nabla \Phi(\mathbf{x}, t)| = 0, \quad \Phi(\mathbf{x}, 0) = \Phi_0(\mathbf{x}), \quad (2)$$

where v_n is the magnitude of normal velocity, and $\Phi_0(\mathbf{x})$ defines the initial model.

For linear elastic structural problem, the classical formulation of mean compliance minimization with volume constraint is defined as:

$$\begin{aligned} \min_{\Phi} \quad & J(\mathbf{u}, \Phi) = \int_{\Omega} \boldsymbol{\epsilon}(\mathbf{u})^T \mathbf{C} \boldsymbol{\epsilon}(\mathbf{u}) d\Omega, \\ \text{s.t.} \quad & V(\Phi) \leq V_{\max} \quad \text{where} \quad V(\Phi) = \int_{\Omega} d\Omega, \end{aligned} \quad (3)$$

where $\mathbf{u} \in \mathbb{R}^d$ is the displacement field, $\boldsymbol{\epsilon}(\mathbf{u})$ the strain field, \mathbf{C} the elasticity matrix, and V_{\max} the volume constraint. To solve this constrained optimization problem, a common technique is to construct an augmented objective

functional by multiplying the volume constraint $V(\Phi)$ with a positive Lagrange multiplier λ :

$$\min_{\Phi} L(\mathbf{u}, \Phi) = \int_{\Omega} \boldsymbol{\epsilon}(\mathbf{u})^T \mathbf{C} \boldsymbol{\epsilon}(\mathbf{u}) d\Omega + \lambda (V(\Phi) - V_{\max}). \quad (4)$$

As derived in Allaire et al. (2004) and Wang et al. (2003), the shape derivative can be obtained by the differentiation of the Lagrangian L with respect to time t :

$$\frac{dL}{dt} = \int_{\partial\Omega} (\lambda - \boldsymbol{\epsilon}(\mathbf{u})^T \mathbf{C} \boldsymbol{\epsilon}(\mathbf{u})) v_n ds. \quad (5)$$

Then, a standard steepest descent search is generally adopted with the magnitude of normal velocity defined as:

$$v_n = -(\lambda - \boldsymbol{\epsilon}(\mathbf{u})^T \mathbf{C} \boldsymbol{\epsilon}(\mathbf{u})). \quad (6)$$

Substituting (6) into (2) and solving the Hamilton–Jacobi equation, the optimal design can be obtained consequently.

Note that, although only the compliance minimization problem is concerned in this paper to demonstrate the effectiveness of the proposed algorithm, extensions to other objectives and constraints (Allaire and Jouve 2008) are straightforward.

2.2 RBF+POU model with dynamic knots

To circumvent the disadvantages arising from the discrete level set method, the RBF based model provides a continuous parametric representation, which replaces the time-dependent $\Phi(\mathbf{x}, t)$ by a series of coefficients α_i and the RBF interpolants φ_i as follows:

$$\Phi(\mathbf{x}, t) = \sum_{i=1}^N \alpha_i \varphi_i(\mathbf{x}, t), \quad (7)$$

where N is the number of RBFs, and the expansion coefficients α_i (positive or negative) are determined from the initial model interpolation and remain constant throughout the optimization process. Similar to the works in Cheng et al. (2003) and Ho et al. (2011), the following function of inverse multiquadric (IMQ) is chosen as the basis function due to the stability and sensitivity concerns:

$$\varphi_i(\mathbf{x}, t) = \frac{1}{\sqrt{|\mathbf{x} - \mathbf{x}_i(t)|^2 + c_i^2}}, \quad (8)$$

where c_i is a constant. It should be noted that each IMQ is an infinitely smooth spline centered at its dynamic knot $\mathbf{x}_i(t)$, where the scalar implicit function $\Phi(\mathbf{x}, t)$ are interpolated.

The POU method (Ho et al. 2011; Ohtake et al. 2003; Tobor et al. 2004a, b) is the other key technique adopted to improve the computational efficiency for the RBF based model. It divides the design domain into numbers of overlapping patches $\{D_i\}_{i=1}^M$ covering the entire domain D such that $D \subseteq \cup_i D_i$ (Fig. 1). Thus, a local RBF model Φ_i can be reconstructed at each subdomain D_i from (7) and (8), and then the global function $\tilde{\Phi}$ is defined by blending all the local interpolants through the following expression:

$$\tilde{\Phi}(\mathbf{x}, t) = \sum_{i=1}^M w_i(\mathbf{x}) \Phi_i(\mathbf{x}, t), \tag{9}$$

where $w_i(\mathbf{x})$ is a collection of the non-negative blending functions. This set of compactly-supported and continuous blending functions are obtained from a set of weight functions W_i by an inverse distance weighting procedure—Shepard’s Method (Griebel and Schweitzer 2000):

$$w_i(\mathbf{x}) = \frac{W_i(\mathbf{x})}{\sum_j W_j(\mathbf{x})}, \tag{10}$$

where it satisfies $\sum w_i(\mathbf{x}) = 1$. The smooth functions W_i have to be continuous at the boundary of the subdomains D_i . It is defined as the composition of a distance function $P_i : \mathbb{R}^n \rightarrow [0, 1]$, where $P_i(x) = 1$ at the boundary of Ω_i , and a decay function $\mathcal{V} : [0, 1] \rightarrow [0, 1]$, i.e. $W_i(\mathbf{x}) = \mathcal{V} \circ P_i(\mathbf{x})$ (Tobor et al. 2004b). For a 3D axis-aligned box defined from the two opposite corners S and T , the distance function P_i is expressed as (Griebel and Schweitzer 2000; Tobor et al. 2004b; Wu et al. 2005):

$$P_i(\mathbf{x}) = 1 - \prod_{r=x,y,z} \frac{4(r - S_r)(T_r - r)}{(T_r - S_r)^2}, \tag{11}$$

where S_r and T_r are the position of S and T in 3D, respectively.

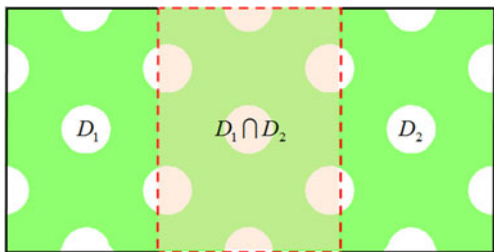


Fig. 1 POU: subdomains D_i constitute the entire domain D

The choice of the decay function \mathcal{V} determines the continuity between the local interpolant Φ_i in the global reconstruction function $\tilde{\Phi}$. In this paper, the following decay functions are suggested for different constraint cases:

$$\begin{aligned} \text{continuity } \mathbb{C}^0 : \mathcal{V}^0(d) &= 1 - d, \\ \text{continuity } \mathbb{C}^1 : \mathcal{V}^1(d) &= 2d^3 - 3d^2 + 1, \\ \text{continuity } \mathbb{C}^2 : \mathcal{V}^2(d) &= -6d^5 + 15d^4 - 10d^3 + 1. \end{aligned} \tag{12}$$

3 Sensitivity analysis and optimization algorithm

3.1 Sensitivity analysis

As the positions of the knots \mathbf{x}_j in each patch Ω_i change with time, (8) can be modified as:

$$\varphi_{ij}(\mathbf{x}, t) = \frac{1}{\sqrt{|\mathbf{x} - \mathbf{x}_j(t)|^2 + c_j^2}}, \tag{13}$$

and the local reconstruction function Φ_i becomes:

$$\Phi_i(\mathbf{x}, t) = \sum_{j=1}^N \alpha_{ij} \varphi_{ij}(\mathbf{x}, t). \tag{14}$$

Substituting (14) into (9) for the global function $\tilde{\Phi}$, the Hamilton–Jacobi equation (2) can be rewritten as:

$$\sum_{i=1}^M w_i \sum_{j=1}^N \alpha_{ij} \frac{\partial \varphi_{ij}(\mathbf{x}, t)}{\partial \mathbf{x}_{ij}} \cdot \dot{\mathbf{x}}_{ij} + v_n |\nabla \tilde{\Phi}| = 0, \tag{15}$$

where

$$\begin{aligned} \nabla \tilde{\Phi} &= \frac{\partial \tilde{\Phi}}{\partial \mathbf{x}_{ij}} \\ &= \sum_i w_i \sum_j \alpha_{ij} \frac{\partial \varphi_{ij}}{\partial \mathbf{x}_{ij}} + \frac{1}{\sum_j W_j} \sum_i \frac{\partial W_i}{\partial \mathbf{x}_i} \cdot (\Phi_i - \tilde{\Phi}). \end{aligned} \tag{16}$$

The normal velocity v_n on the moving boundary can be obtained consequently by rewriting (15) as:

$$v_n = \frac{1}{|\nabla \tilde{\Phi}|} \sum_{i=1}^M w_i \sum_{j=1}^N \alpha_{ij} \frac{\partial \varphi_{ij}(x, t)}{\partial \mathbf{x}_{ij}} \cdot \dot{\mathbf{x}}_{ij}. \tag{17}$$

Then, by substituting (17) into (5), the shape derivative in term of x_{ij} appears as:

$$\begin{aligned} \frac{dL}{dt} &= \sum_{i=1}^M \sum_{j=1}^N \alpha_{ij} \int_{\partial \Omega} (\lambda - \epsilon(u)^T \mathbf{C} \epsilon(u)) \frac{1}{|\nabla \tilde{\Phi}|} w_i \\ &\quad \cdot \frac{\partial \varphi_{ij}(x, t)}{\partial \mathbf{x}_{ij}} ds \cdot \dot{\mathbf{x}}_{ij}, \end{aligned} \tag{18}$$

Table 1 Optimization algorithm

- 1: Choose initial $\tilde{\Phi}_0 \in D$, set $n = 0$.
- 2: Compute the initial RBF basis function φ^0 of Ω^0 .
- 3: **repeat**
- 4: Compute \mathbf{u}^n of Ω^n using FEM.
- 5: Solve the descent gradient $\frac{\partial J}{\partial \mathbf{x}_{ij}}, \frac{\partial V}{\partial \mathbf{x}_{ij}}$ from (20) and (21).
- 6: Evaluate the search direction $\dot{\mathbf{x}}_{ij}$ in (22).
- 7: Update the position of knots \mathbf{x}_{ij}^{n+1} by (23).
- 8: Update the RBF basis function φ^n .
- 9: Update level set function $\tilde{\Phi}^{n+1}$ by (24).
- 10: Update shape Ω^{n+1} .
- 11: $n++$.
- 12: **until** $\|J(\tilde{\Phi}^{n+1}) - J(\tilde{\Phi}^n)\| < \epsilon$.

On the other hand, the following derivative can also be obtained by chain rule as:

$$\begin{aligned} \frac{dL}{dt} &= \sum_{i=1}^M \sum_{j=1}^N \frac{\partial L}{\partial \mathbf{x}_{ij}} \cdot \dot{\mathbf{x}}_{ij} \\ &= \sum_{i=1}^M \sum_{j=1}^N \frac{\partial J}{\partial \mathbf{x}_{ij}} \cdot \dot{\mathbf{x}}_{ij} + \lambda \sum_{i=1}^M \sum_{j=1}^N \frac{\partial V}{\partial \mathbf{x}_{ij}} \cdot \dot{\mathbf{x}}_{ij}. \end{aligned} \tag{19}$$

Therefore, as shown in (18) and (19), the sensitivities of the objective function and the volume constraint can be derived by comparing them in the following way:

$$\begin{aligned} \frac{\partial J}{\partial \mathbf{x}_{ij}} &= -\alpha_{ij} \int_{\partial\Omega} \boldsymbol{\epsilon}(u)^T \mathbf{C} \boldsymbol{\epsilon}(u) \frac{1}{|\nabla \tilde{\Phi}|} w_i \frac{\partial \varphi_{ij}}{\partial \mathbf{x}_{ij}} ds, \\ i &= 1, \dots, N; \quad j = 1, \dots, M, \end{aligned} \tag{20}$$

$$\begin{aligned} \frac{\partial V}{\partial \mathbf{x}_{ij}} &= \alpha_{ij} \int_{\partial\Omega} \frac{1}{|\nabla \tilde{\Phi}|} w_i \frac{\partial \varphi_{ij}}{\partial \mathbf{x}_{ij}} ds, \\ i &= 1, \dots, N; \quad j = 1, \dots, M. \end{aligned} \tag{21}$$

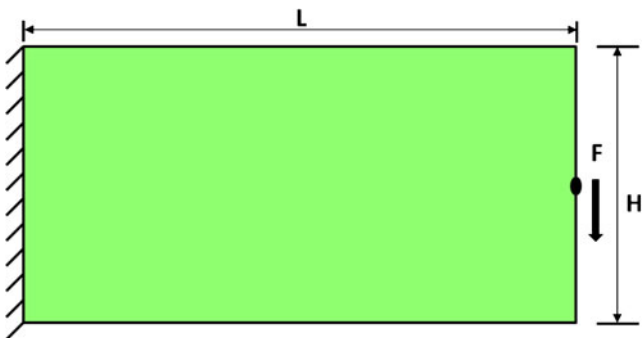
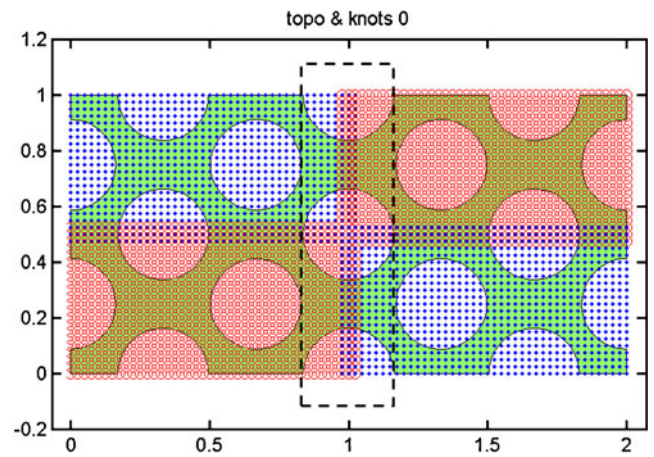
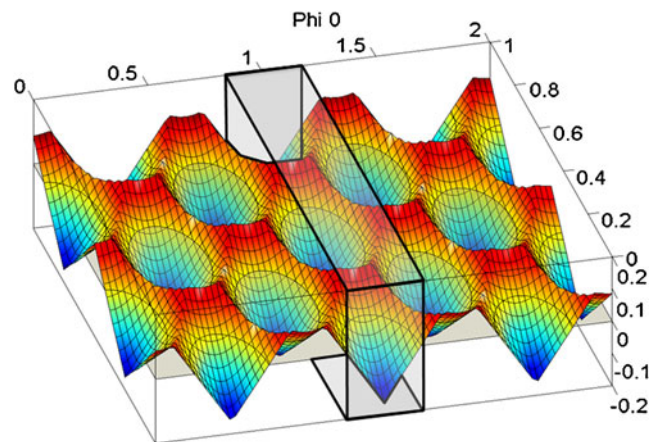


Fig. 2 Design domain: cantilever beam with dimension $L : H = 2 : 1$



(a) 2D plot with overlapping knots



(b) 3D contour plot of $\varphi(x)$

Fig. 3 Patch pattern of Case 1b

3.2 Optimization algorithm

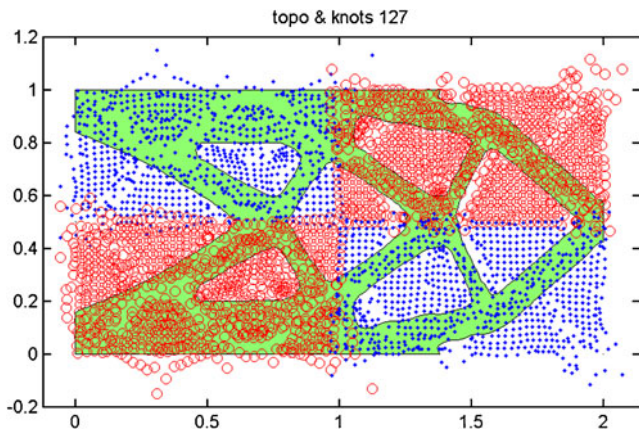
Table 1 lists the detailed optimization algorithm. To find the local minimum of the objective function as stated in (3), the steepest descent method is employed to proceed with the search in the descent direction of the sensitivity functions

Table 2 Comparison of results for Case 1

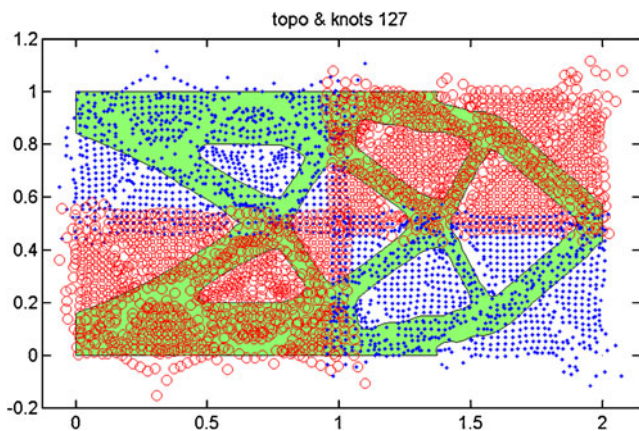
Case no.	Overlap size $n_x \times n_y$	Patch pattern	Total no. knots	Time/step (s)	Compliance
1a	41 × 21	2 × 2	3444	6.83	60.6
2b	42 × 22	2 × 2	3696	7.12	60.4
3c	43 × 23	2 × 2	3956	7.32	61.7

at the current point. From (19) the search direction can be defined as:

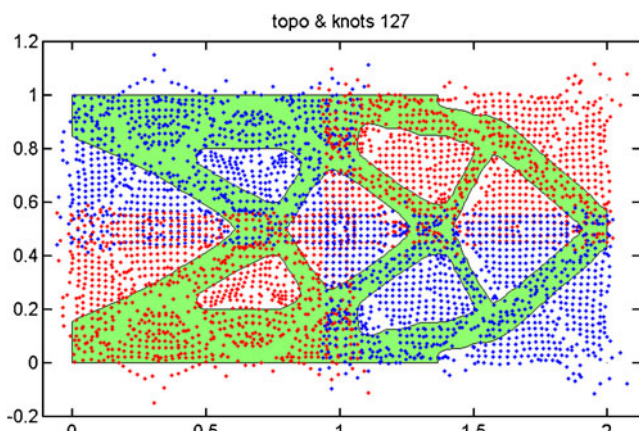
$$\dot{\mathbf{x}}_{ij} = - \left(\frac{\partial J}{\partial \mathbf{x}_{ij}} + \lambda \frac{\partial V}{\partial \mathbf{x}_{ij}} \right), \quad i = 1, \dots, N; \quad j = 1, \dots, M, \tag{22}$$



(a) CASE 1a



(b) CASE 1b



(c) CASE 1c

Fig. 4 Optimization step 127 of Case 1

Table 3 Comparison of results for Case 2a

Case no.	Patch pattern	Total no. knots	Time/step (s)	Compliance	Volume fraction
i	1 × 2	3362	8.05	60.4	0.499
ii	1 × 4	3444	6.96	60.5	0.499
iii	1 × 5	3485	6.69	61.0	0.498
iv	1 × 8	3608	6.41	61.1	0.499
v	1 × 10	3690	6.29	60.8	0.499

Table 4 Comparison of results for Case 2b

Case no.	Patch pattern	Total no. knots	Time/step (s)	Compliance	Volume fraction
i	2 × 1	3402	7.95	60.5	0.499
ii	4 × 1	3564	6.87	60.8	0.499
iii	5 × 1	3645	6.69	60.5	0.498
iv	8 × 1	3888	6.49	60.8	0.499
v	10 × 1	4050	6.35	60.7	0.499

Table 5 Comparison of results for Case 2c

Case no.	Patch pattern	Total no. knots	Time/step (s)	Compliance	Volume fraction
i	2 × 2	3444	6.86	60.4	0.499
ii	4 × 4	3696	6.07	60.5	0.499
iii	5 × 5	3825	5.98	61.0	0.498
iv	8 × 8	4224	5.93	61.1	0.499
v	10 × 10	4500	5.93	60.8	0.499

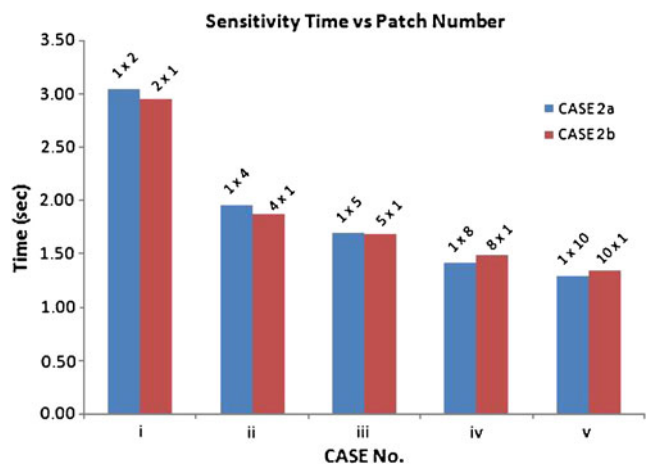


Fig. 5 Plot of sensitivity time vs patch number for Cases 2a and 2b

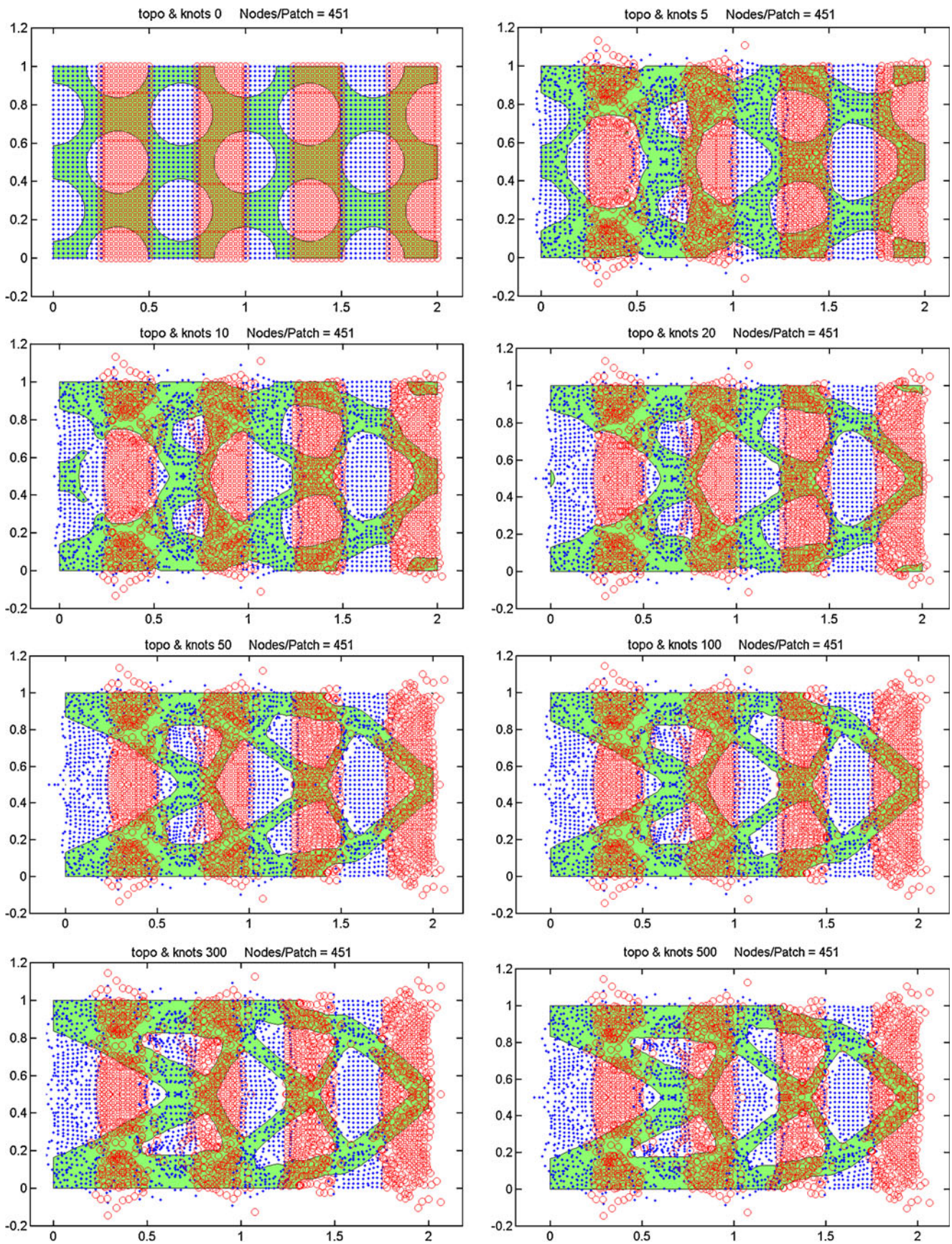


Fig. 6 Optimization steps of Case 2a(iv): patch pattern $(P_y \times P_x) = 1 \times 8$, total knots number = 3608, time consumed per iteration = 6.41 s

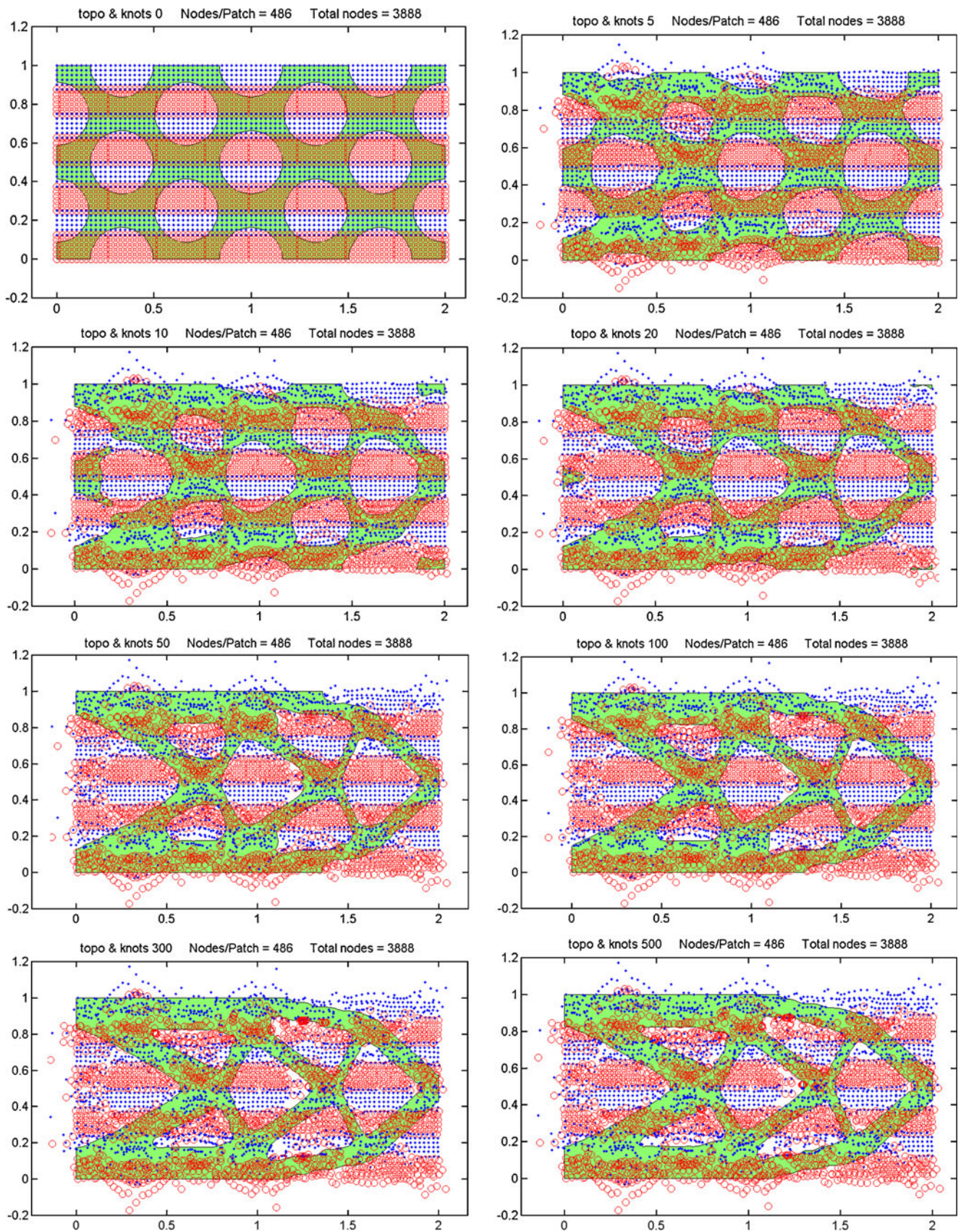


Fig. 7 Optimization steps of Case 2b(iv): patch pattern $(P_y \times P_x) = 8 \times 1$, total knots number = 3888, time consumed per iteration = 6.49 s

and the position of knots \mathbf{x}_{ij} can be updated as:

$$\mathbf{x}_{ij}^{n+1} = \mathbf{x}_{ij}^n + \tau \dot{\mathbf{x}}_{ij}, \quad i = 1, \dots, N; \quad j = 1, \dots, M, \quad (23)$$

where τ is the fixed time step.

Once the knot position is updated as \mathbf{x}_{ij}^{n+1} , it is substituted into (13) and (14) to get the updated local interpolant. Then, the new level set function can be deduced from (9) as:

$$\tilde{\Phi}^{n+1} = \sum_{i=1}^M w_i \sum_{j=1}^N \alpha_{ij} \varphi_{ij}^{n+1}. \quad (24)$$

Thus, the implicit function is computed everywhere in the domain and the boundary of the structure is propagated accordingly.

4 Numerical results

In this section, the optimization problem (3) is concerned, and a benchmark example of a short cantilever beam is utilized to analyze the proposed algorithm with different settings. As shown in Fig. 2, a point load $F = 1$ is applied at the middle of the right end, meanwhile a fixed boundary condition is imposed on the left side. The structure is discretized with a rectilinear mesh of 80×40 elements, and the size of each element is $h = 0.025$. The volume fraction is $\zeta = 50\%$ of the design domain, and the time step is $t_\tau = 5 \times 10^{-3}$. For finite element analysis, the “ersatz material” method (Allaire et al. 2004) is adopted, for which a weak material with Young’s modulus $E = 10^{-3}$ is assumed in void region (i.e. holes), and $E = 1$ for solid material. Specifically, for an element containing solid material of density ρ_e , its stiffness K_e is defined as: $K_e = \rho_e \times K_s$, where K_s is the stiffness of a fully occupied element. To evaluate the boundary integral of the sensitivities (20) and (21), a standard Gaussian integration (Wei and Wang 2006) is performed over the zero-level contour of the level-set function. In the implementation, three sampling points are employed over a boundary segment inside an element. In addition, the second decay function in (12) of continuity C^1 is implemented, and stopping threshold $\epsilon = 10^{-6}$ is set.

4.1 Case 1—Effect of the amount of overlapping knots

The first experiment is to study the effect of the overlapping knots. It is because the size of the overlapping regions of the adjacent patches may impose different effects on the Shepard functions w_i and may cause very large gradient of w_i close to the boundary of the respective support Ω_i . In result, the accuracy of the global approximation $\tilde{\Phi}$ may be jeopardized by the insufficient representation.

In this test, three overlapping configuration settings are studied: (a) 1-knot, (b) 3-knots and (c) 5-knots in both directions of the rectangular patch (i.e. n_x and n_y). Figure 3a depicts the initial patch configuration of Case 1b, and the corresponding Φ is plotted in Fig. 3b. The overlapping regions between the patches are reconstructed smoothly using the proposed method. Table 2 summarizes the different cases and the corresponding computation time.

It is straightforward to understand that the computational time is directly related to the number of the overlapping knots, because the scale of the coefficient matrix of RBF interpolation enlarges as the amount of knots increases. As shown in Table 2, Case 1a scores the shortest computational time, for which there is only one knot situated in the overlapping region.

Nonetheless, from the observation of the optimization process, the rate of the topological change of the three cases are almost the same. Figure 4 captures the configurations at design iteration 127, which shows that the topology of all the designs are very similar.

This evidence implies that the amount of the overlapping knots decides the computational efficiency, but it does not apply any noticeable impact on the simulation result. Therefore, the overlapping region with one knot from the neighboring patch is sufficient. Besides, the final optimal designs also reveal that the boundaries of D_i can be well represented by the Shepard function w_i and thus the accuracy of the global approximation $\tilde{\Phi}$ is maintained in a good condition.

4.2 Case 2—Effect of the patch pattern

The second study focuses on the effect of the patch pattern ($P_y \times P_x$) to the simulation result and overall efficiency, where P_x and P_y denote the number of patches in x- and y-direction respectively. Note that the 1-knot overlapping condition is adopted here for efficiency concern as concluded from Case 1.

As a comparison, the domain is divided into patches in x-direction only (Case 2a), y-direction only (Case 2a),

Table 6 Comparison of results for Case 2d

Case no.	Patch pattern	Total no. knots	Time/step (s)	Compliance	Volume fraction
i	5×10	4050	5.92	60.6	0.500
ii	10×5	4250	5.94	60.6	0.500
iii	10×20	5000	5.99	61.4	0.500
iv	20×10	5400	6.01	61.2	0.500
v	20×20	6000	6.14	62.3	0.500
vi	20×40	7200	6.50	94.3	0.500

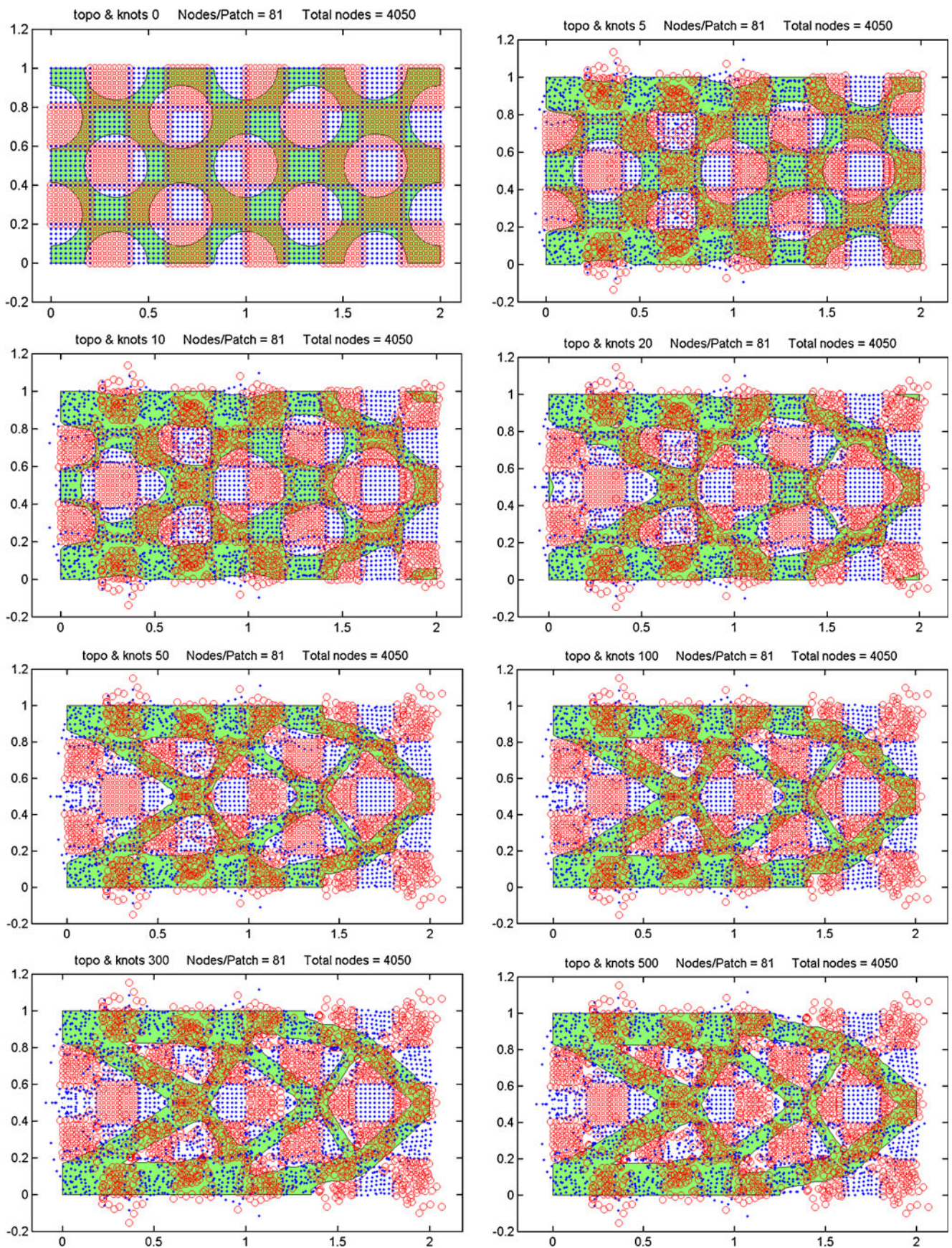
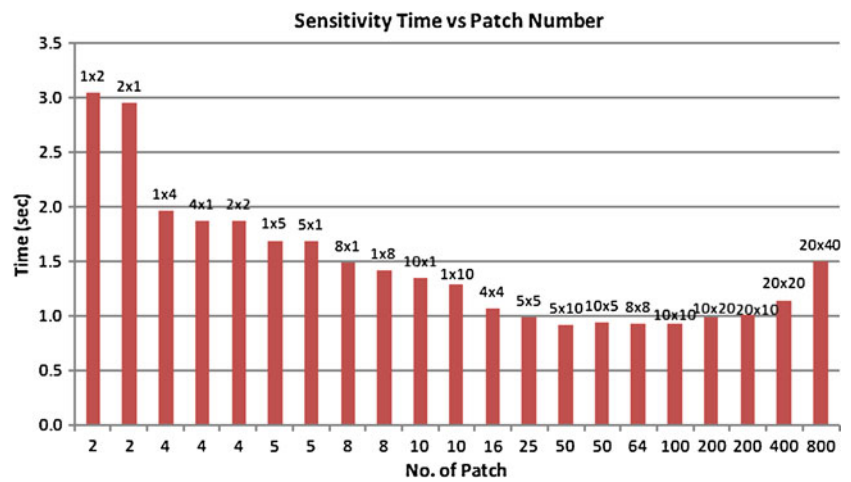


Fig. 8 Optimization steps of Case 2d(i): patch pattern $(P_y \times P_x) = 5 \times 10$, total knots number = 4050, time consumed per iteration = 5.92 s

Fig. 9 Plot of sensitivity time vs patch number



and both x- and y-directions (Case 2c). For each case, there are five model settings to be evaluated, and all the simulations stops at iteration 500 unless it converges beforehand. The corresponding experimental data are tabulated in Tables 3, 4 and 5 respectively. Remarkably, the computational cost of each case drops proportionally as the number of patches and overlapping knots increases, and the final optimal designs have little differences from each other with similar compliance values.

Note that for each design iteration, the main computational effort consists of three parts: (1) finite element analysis (FEM), (2) sensitivity analysis, and (3) model updating. Because the processes (1) and (3) are determined by the discretized grid which is the same for all the test cases, comparison on the computational cost of process (2) may reveal the truth. Hence, Fig. 5 plots the computational time of the “sensitivity analysis” against the number of patch for Cases 2a and 2b. The differences between these two cases are less than 2 % in terms of number of knots and sensitivity time. However, the result shows that the computation time

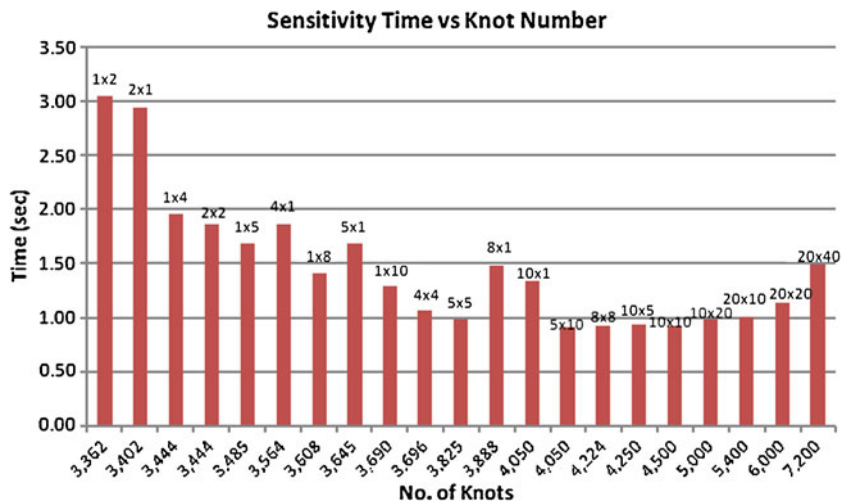
is mainly governed by the number of patch if the difference in the knot amount is not significantly large.

In addition, Figs. 6 and 7 illustrate the simulation of Case 2a(iv) [1 × 8] and Case 2b(iv) [8 × 1] in details. The results ensure that the POU method does not impose significant quality problem onto the accuracy of the calculation. Besides, the boundary propagations in both cases are very close and the final topologies are approximately the same.

Theoretically, a contradiction exists between the number of patches and knots towards the efficiency of optimization, because more patches result in a smaller scale of interpolation matrix but bring more overlapping knots to be considered. Therefore, in order to further study the efficiency issue against the number of patches and knots, the last Case 2d is performed to accommodate more patch combinations and knots. The details of the model settings are listed in Table 6.

In Case 2d(i) [5 × 10], it finishes an iteration in 5.92 s which is the quickest in this study, and the total number of

Fig. 10 Plot of sensitivity time vs knot number



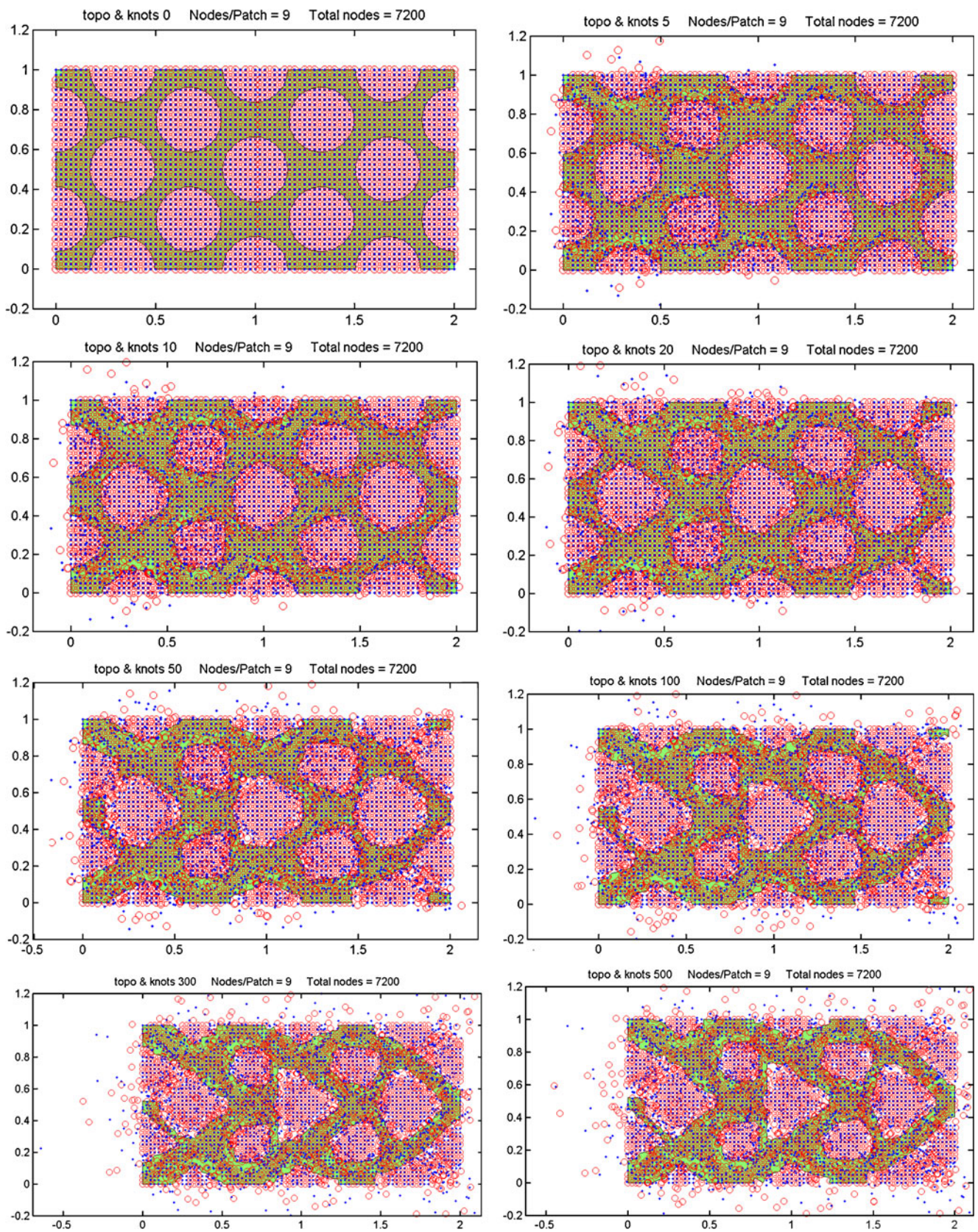


Fig. 11 Optimization steps of Case 2d(vi): patch pattern $(P_y \times P_x) = 20 \times 40$, total knots number = 7200, time consumed per iteration = 6.50 s

patches and knots are 50 and 4050, respectively. As shown in the Fig. 8, the final result converges to the similar topology obtained from the typical dynamic knots scheme as well. The overviews of the comparison results are given in the Fig. 9 (number of patch vs sensitivity time) and Fig. 10 (number of knot vs sensitivity time). The results show that when the number of patches exceed 100, the sensitivity time increases even if the patch number is still increasing. It is because the density of the overlapping knots become significant such that the computational speed slows down eventually. In Case 2d(vi), the numbers of patches and knots are the highest. However, the over-populated knots span deteriorates the simulation quality, and the optimization process does not converge as shown in Fig. 11.

5 Conclusion

In this paper, an effective structural optimization scheme is proposed by combining the dynamics knots with the RBF+POU based parametric model representation.

Numerical experiments reveal that the POU method is stable against different arrangements of the patch patterns, and the computational efficiency is directly proportional to the number of patches. However, proper deployment of patches and overlapping knots plays a key role on the performance. In fact, there is no need to place large amount of knots in the overlapping region, because the combination of the continuous function φ_i and the compactly supported shape function w_i provide a sufficient representation over the whole domain. Otherwise, the overall performance may be dragged down due to large interpolation matrix. In addition, the best patch deployment is obtained in Case 2d(i), for which each patch covers a region of 2×2 grid elements. Therefore, as long as the number of patches and knots is in a reasonable ratio, the proposed scheme can reduce the computation time.

It is also worthy noted that compactly supported RBF method has the same advantage to the POU method in reducing the computational burden. However, due to the local influence nature of compactly supported basis function, it is possible that certain design domain may not be covered or supported after arbitrarily moving the knots. Therefore, it is dangerous to directly apply the algorithm proposed in this paper for compactly supported RBF method. Instead, a careful optimization strategy shall be derived to prevent such phenomenon, which is hopefully a promising research topic.

Nonetheless, the current numerical scheme is by no means complete. To extend it to three dimensional design with practical engineering problems is targeted as the future work. One promising area is the multi-material microstructure design of multi-physics, such as designing materials

with unusual properties, like negative Poisson's ratio and zero thermal expansion coefficient (Bendsøe and Sigmund 2003). It would be informative to compare the results of the proposed approach with the homogeneous method and discrete level set method.

Acknowledgement This research work is supported by the Research Grants Council of Hong Kong SAR (Project No. CUHK417309).

References

- Allaire G, Jouve F, Toader A-M (2004) Structural optimization using sensitivity analysis and a level-set method. *J Comput Phys* 194(1):363–393
- Allaire G, Jouve F (2008) Minimum stress optimal design with the level set method. *Eng Anal Bound Elem* 32(11):909–918
- Bendsøe MP (1989) Optimal shape design as a material distribution problem. *Struct Multidisc Optim* 1:193–202
- Bendsøe MP, Kikuchi N (1988) Generating optimal topologies in structural design using a homogenization method. *Comput Methods Appl Mech Eng* 71:197–224
- Bendsøe MP, Sigmund O (2003) *Topology optimization: theory, methods and applications*, 2nd edn. Springer, Berlin
- Buhmann MD (2004) *Radial basis functions: theory and implementations*. In: Cambridge monographs on applied and computational mathematics, vol 12. Cambridge University Press, New York
- Cheng AD, Golberg MA, Kansa EJ, Zammuto G (2003) Exponential convergence and h -c multiquadric collection method for partial differential equations. *Numer Methods Partial Differ Equ* 19: 571–594
- Ho HS, Lui BFY, Wang MY (2011) Parametric shape and topology optimization with radial basis functions and partition of unity method. *Optim Methods Softw* 26(4–5):533–553
- Griebel M, Schweitzer MA (2000) A particle-partition of unity method for the solution of elliptic, parabolic, and hyperbolic pdes. *SIAM J Sci Comput* 22:853–890
- Lui BFY, Wang MY, Xia Q (2007) Parametric shape and topology optimization via radial basis functions, partition of unity and level set method. In: Proceedings of 5th China–Japan–Korea joint symposium on optimization of structural and mechanical systems. Jeju, Korea
- Luo Z, Wang MY, Wang SY, Wei P (2007) A level set-based parameterization method for structural shape and topology optimization. *Int J Numer Methods Eng* 76(1):1–26
- Ohtake Y, Belyaev A, Alexa M, Turk G, Seidel HP (2003) Multi-level partition of unity implicits. In: Proceedings of ACM SIGGRAPH 2007 (SESSION: Surfaces), pp 463–470
- Rozvany GIN, Zhou M, Birker T (1992) Generalized shape optimization without homogenization. *Struct Multidisc Optim* 4(3–4): 250–252
- Tobor I, Reuter P, Schlick C (2004a) Efficient reconstruction of large scattered geometric datasets using the partition of unity and radial basis functions. *J WSCG* (12):467–474
- Tobor I, Reuter P, Schlick C (2004b) Multi-scale reconstruction of implicit surfaces with attributes from large unorganized point sets. In: Proceedings of shape modeling applications, pp 19–30
- Wang SY, Wang MY (2006) Radial basis functions and level set method for structural topology optimization. *Int J Numer Methods Eng* 65:2060–2090
- Wang MY, Wang XM, Guo DM (2003) A level set method for structural topology optimization. *Comput Methods Appl Mech Eng* 192:227–246

- Wei P, Wang MY (2006) Parametric structural shape and topology optimization method with radial basis functions and level-set method. In: Proceedings of IDETC/CIE, pp 19–30
- Wu X, Wang MY, Xia Q (2005) Implicit fitting and smoothing using radial basis functions with partition of unity. In: Proceedings of the ninth international conference (2005) on computer aided design and computer graphics, pp 139–148
- Xie YM, Steven GP (1993) A simple evolution procedure for structural optimization. *Comput Struct* 49(5):885–896
- Xie YM, Steven GP (1997) *Evolutionary structural optimization*. Springer, New York
- Xing XH, Wang MY, Lui BFY (2007) Parametric shape and topology optimization with moving knots radial basis functions and level set methods. In: Proceedings of the 7th WCSMO, pp 1928–1936